The International Journal of Advanced Manufacturing Technology (2019) 102:487–496
https://doi.org/10.1007/s00170-018-3195-z

ORIGINAL ARTICLE

Research on the matching relationship between ultrasonic-assisted grinding parameters and workpiece surface roughness

Siyuan Sun[1] · Jinyuan Tang[1] · Wen Shao[1] · Changshun Chen[1] · Yaoxi Liu[1]

Received: 12 June 2018 / Accepted: 12 December 2018 / Published online: 4 January 2019

Abstract

As a nontraditional type of processing technology, ultrasonic-assisted grinding (UAG) can effectively improve the surface integrity. A considerable research effort has been devoted to investigate the impact of various processing parameters on surface roughness. However, few studies have been conducted on the effects of matching relationship between different parameters. In this study, the numerical model of a dressed grinding wheel is constructed using a measured diamond pen. Based on the grinding kinematics, the micro surface topography of the workpiece is generated. The relationship between surface roughness and three main processing parameters is studied, and the concept of critical ultrasonic amplitude is proposed. It is found that the ultrasonic grinding can effectively weaken the deterioration of the roughness by increasing the depth of cut, and then, the relationship between the critical ultrasonic amplitude and the depth of cut is obtained. Furthermore, the coupling relation is explained from the angle of a single abrasive grain. Finally, the accuracy of the findings is verified by the experimental results, which may serve as an effective method or reference for the setting of ultrasonic grinding parameters.

Keywords Ultrasonic-assisted grinding · Processing parameters · Matching relationship · Critical ultrasonic amplitude

1 Introduction

The integrity of the machined surface such as force, temperature, surface topography, residual stress, microstructure, and microhardness is a subject-driven tremendous scientific interest as these parameters directly influence the tool wear, quality, and even fatigue life of the machined assemblies [1–6]. Among these performance parameters, surface topography exerts an enormous function on the functional behavior such as tribological, wear, and lubrication behaviors of engineering components [7, 8]. As a widely used surface evaluation index, surface roughness is closely related to the processing parameters in the grinding process [9, 10]. Efficient manufacturing of surfaces with lower roughness or better quality is essential to the scientific community and manufacturing industries. Over the years, extensive experimental studies have shown that axial ultrasonic-assisted grinding (UAG) can effectively improve the workpiece surface integrity [11–15].

Tawakoli and Azarhoushang [11, 12] investigated the effects of feed rate and depth of cut on the workpiece surface roughness. It was found that the sinusoidal trajectory of the abrasive grain cutting edge could lead to significant improvement on the surface roughness. Nik et al. [13] studied the effects of the wheel speed and coolant flow rate on surface roughness and grinding force. They found that UAG could expand the contact area between the coolant and the workpiece to improve the surface quality. However, most of the previous studies for UAG have been focused on the investigation of the influence of individual parameters on the surface quality.

Wang et al. [16, 17] presented an optimization model based on grinding kinematics to choose proper machining parameters in ultrasonic-assisted grinding for hard and brittle materials. Chen [18] found that the workpiece surface quality was excellent when the ultrasonic amplitude was one fourth of the dressing lead. These studies indicated that the optimization of roughness under UAG must take the matching relationship between the processing parameters into account.

Currently, the prediction of grinding surface roughness is achieved mainly through theoretical and empirical models. The empirical model only applies to specific

✉ Wen Shao
shaowen_2013@163.com

[1] State Key Laboratory of High Performance Complex Manufacturing, School of Mechanical and Electrical Engineering, Central South University, Changsha 410083, Hunan, China

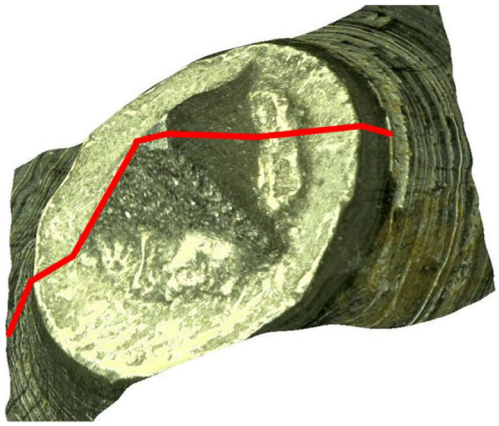

Fig. 1 3D morphology of the single-point diamond pen

conditions, and thus, the relationship between various parameters has no practical physical meaning. The theoretical or numerical methods offer the advantages of yielding a great number of results in a short period, optimizing a comprehensive manufacturing system with sufficiently large sample of data sets, and sometimes providing useful insight into different stages of machining processes [19–22]. The theoretical model developed in this study can effectively simulate the trajectories of abrasive grains and deepen our understanding of the grinding mechanism.

Studies have revealed that the depth of cut plays a significant role in the grinding surface quality in UAG [11, 12]. The magnitude of the ultrasonic amplitude affects the removal of the workpiece material. Meanwhile, a large number of scholars [23–26] found that the dressing lead had a great effect on the grinding wheel surface which is mapped to the workpiece surface through the relative movement between grinding wheel and workpiece. The investigation of matching relationship of three processing parameters, including depth of cut, ultrasonic amplitude, and dressing lead is the main focus of this study.

It is known from the above literature that numerous researches have been conducted to investigate the relationship between the machining parameters and the workpiece surface quality under UAG, but there are still some shortcomings: (1) Previous studies only focus on the effect of a single processing parameter on ultrasonic grinding surface roughness, ignoring the relationship between different processing parameters; (2) most of the researches study the relationship between various parameters through experiments rather than through analytical and numerical techniques.

In this paper, the grinding wheel morphology is first constructed based on the randomly distributed abrasive grains and the measured single-point diamond pen considering the dressing kinematics. Then, the grinding workpiece surface roughness is obtained by taking into the grinding wheel and main machining parameters to study and theoretically explain the coupling matching relationship between the parameters under UAG. Finally, the conclusion of theoretical research is verified and analyzed by UAG experiments.

2 A grinding wheel model for ultrasonic-assisted grinding

The reasonable construction of the grinding wheel is the prerequisite for the accurate prediction of the ultrasonic

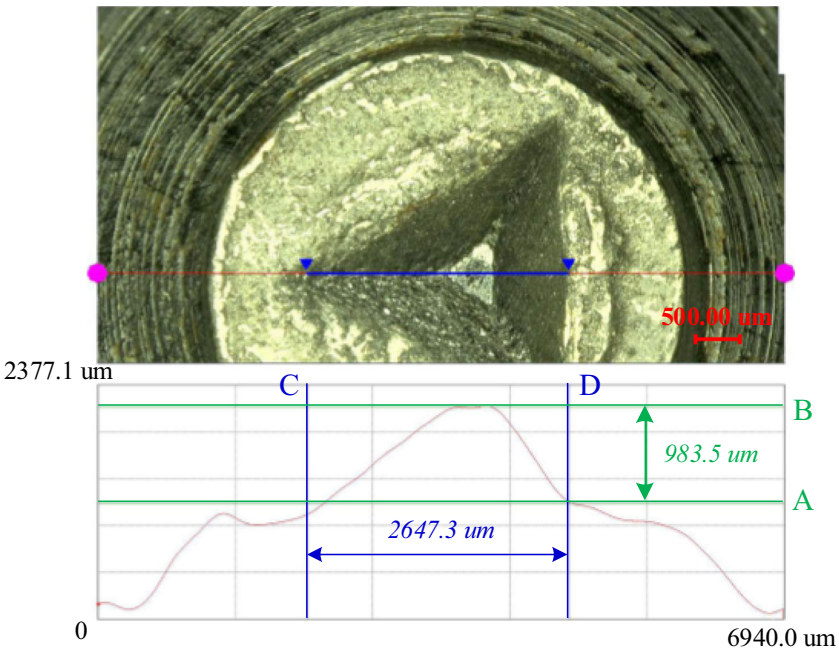

Fig. 2 Height data of the single-point diamond pen

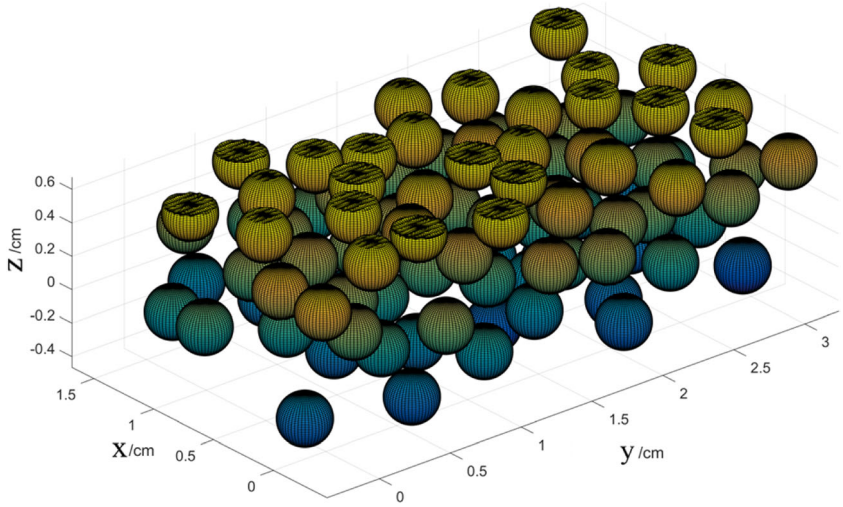

Fig. 3 Numerical model of dressed grinding wheel

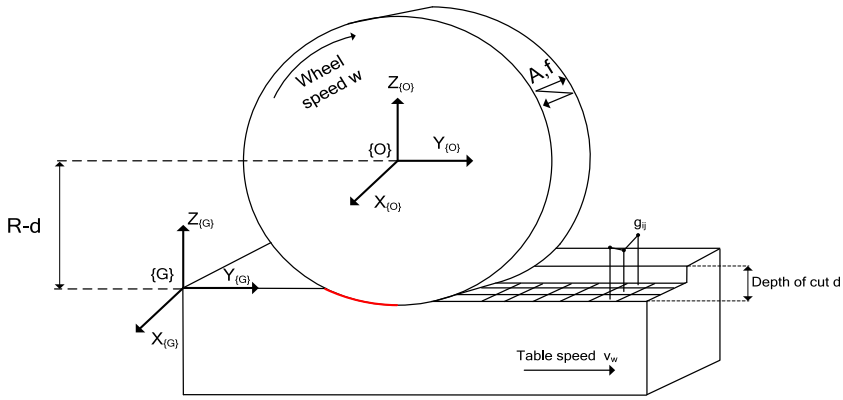

Fig. 4 Schematic of surface grinding process

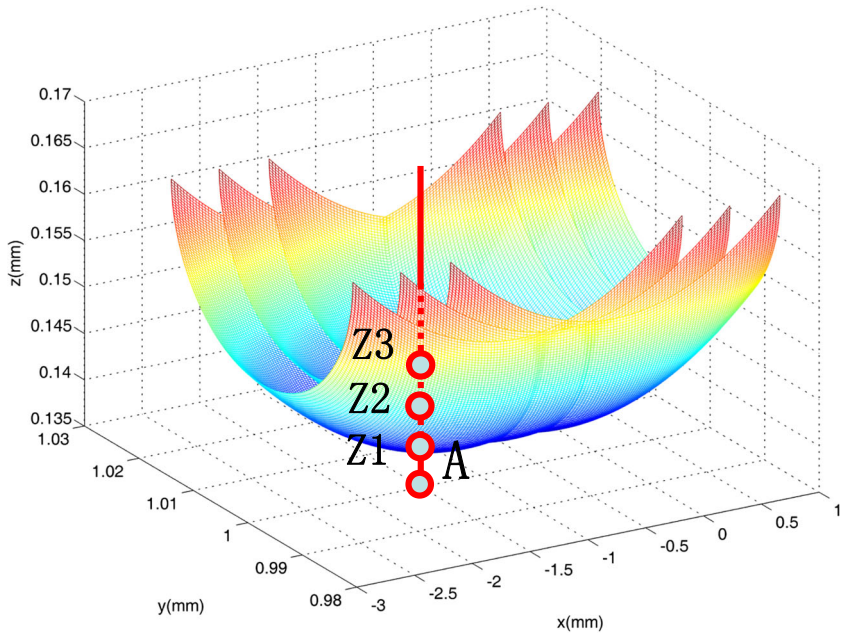

Fig. 5 Schematic of the method for the generation of workpiece surface

Table 1 Major machining parameters

Grinding wheel	Aluminum oxide WA46L
Workpiece	C45 carbon steel (18 mm × 18 mm × 20 mm)
Grinding conditions	Wheel velocity 26 m/s; feed rate 4 m/min; depth of cut $d = 0.02$ mm
Dressing conditions	Wheel velocity 26 m/s; dressing lead $f_d = 0.05$–$0.06 - 0.07$ mm/R; total depth of dressing $a_{d-\text{total}} = 0.1$ mm
Grinding process	Surface grinding
Coolant	120 L/min, Emulsion (Castrol Syntilo 2000)
Direction of ultrasonic vibration	Cross-feed direction
Ultrasonic vibration conditions	Frequency $f = 20$ kHz, amplitude $A = 0$–20 μm
Grinding machine	Mechanical surface grinding machine M7130

grinding workpiece surface roughness. Therefore, it is necessary to construct an accurate grinding wheel to study the coupling relationship between ultrasonic grinding processing parameters and workpiece surface roughness.

The undressed grinding wheel morphology was built according to the references [26, 27]. The grain dimension d_g follows the relationship below

$$d_{\text{gamx}}(\text{mm}) = 15.2M^{-1} \quad (1-1)$$

where M is the grit number.

The average grain dimension can be approximated by

$$d_{\text{gavg}}(\text{mm}) = 68M^{-1.4} \quad (1-2)$$

The grain dimension is found to obey the Gaussian distribution, and the mean value μ can be calculated as

$$\mu = d_{\text{gavg}} \quad (1-3)$$

The standard deviation σ can be estimated as

$$\sigma = \left(d_{gmax} - d_{gavg}\right)/3 \quad (1-4)$$

To generate the topography, the grinding wheel is meshed with a grain interval. The grain interval is the distance between two adjacent grains, and it is related to the structure number S of the wheel. The grain interval Δ (mm) can be determined as

$$\Delta = 137.9M^{-1.4}\sqrt{\frac{\pi}{32-S}} \quad (1-5)$$

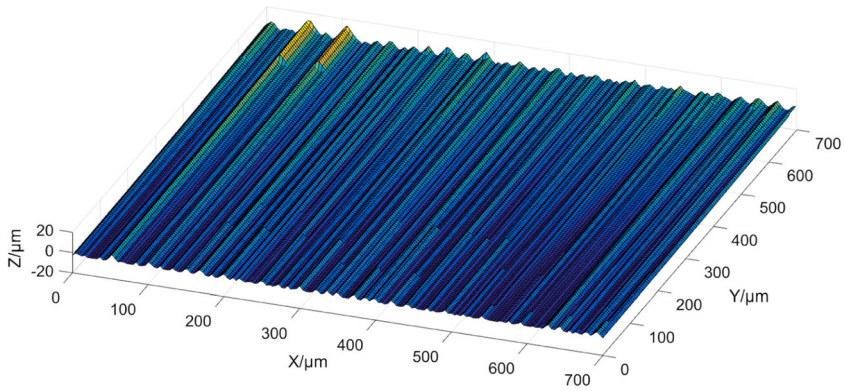

Fig. 6 Grinding workpiece surface obtained at $f_d = 60$ μm/r, $A = 0$ μm, and depth of cut = 20 μm

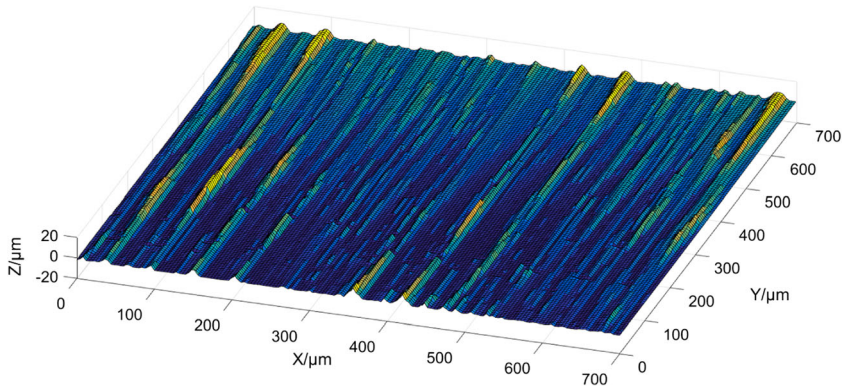

Fig. 7 Grinding workpiece surface obtained at $f_d = 50$ μm/r, $A = 6$ μm, and depth of cut = 11 μm

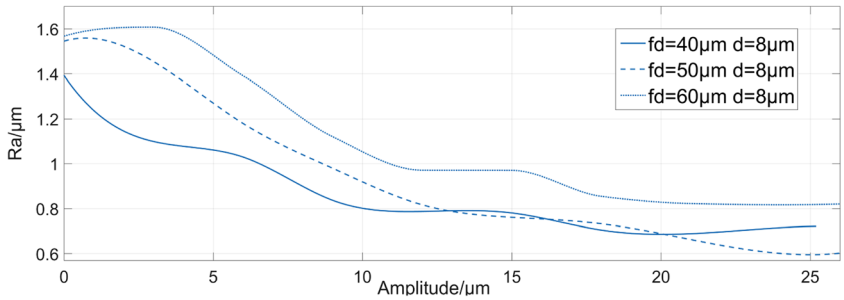

Fig. 8 Variations of surface roughness under different dressing leads ($d = 8$ μm)

With the above parameters, the grinding wheel surface with randomly distributed abrasive grains can be obtained. The morphology of the single-point diamond pen was measured by the LSM 700 laser scanning confocal microscope (CLSM). Figure 1 shows the 3D morphology of a single-point diamond pen. Figure 2 shows the height data of the red line in Fig. 1, which is simplified into a truncated top triangle with a slope of 0.91.

According to Malkin [28], the axial feed of the dresser for each revolution of the grinding wheel is called a dressing lead, which is regarded as the most important dressing parameter for the grinding wheel in the coupling matching relationship. It is derived as

$$f_d = \frac{\pi d_s v_d}{v_s} \qquad (1-6)$$

where v_d is the feed rate of the dresser in the axial direction of the grinding wheel, v_s is the speed of the grinding wheel, and d_s is the diameter of the grinding wheel.

The grit and structure numbers of the simulated grinding wheel are 46 and 8, respectively. According to the relative movement of the single-point diamond pen and the grinding wheel, the numerical model of the grinding wheel with a dressing lead of 50 μm is obtained, as shown in Fig. 3.

3 UAG workpiece surface generation model

In order to establish the trajectory of the abrasive grains under axial ultrasonic-assisted grinding, two coordinate systems are used to describe the grinding motion. One is the local coordinate system {O} which is fixed in the center of the grinding wheel at one side, and the other is fixed on the workpiece surface {G}. These coordinate systems are initially separated by distances of 0, 0, and (*R*-*d*) along the *X*-, *Y*- and Z-axes, respectively.

An array of height [h_{nm}] represents the surface of grinding wheel with the subscripts *m* and *n* corresponding to the posi-

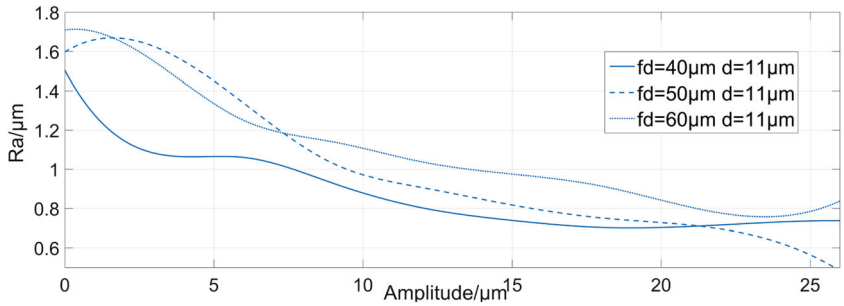

Fig. 9 Variations of surface roughness under different dressing leads ($d = 11$ μm)

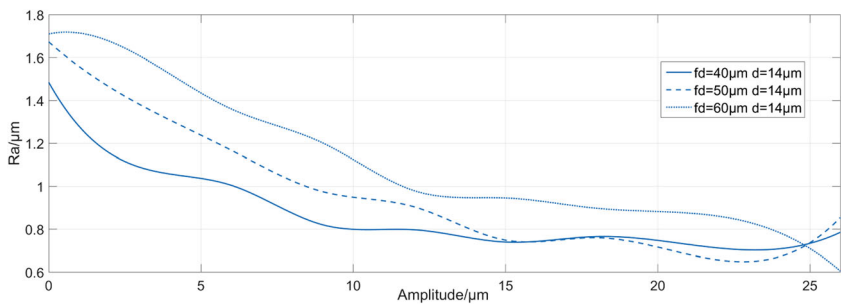

Fig. 10 Variations of surface roughness under different dressing leads ($d = 14$ μm)

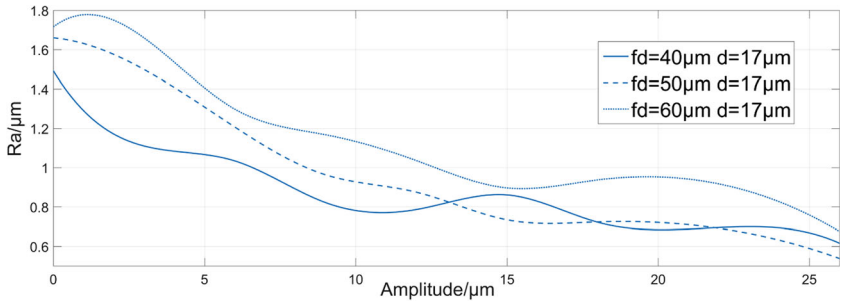

Fig. 11 Variations of surface roughness under different dressing leads ($d = 17$ μm)

tion of the grain protrusion height in the axial and peripheral directions of the wheel. The envelope of the grinding trajectory at any time under the local coordinate system {O} can be transformed to the coordinate system {G} (the sign is negative when the process is up-grinding). The trajectories of the abrasive grains in the coordinate system {G} can be expressed as

$$\begin{cases} x = x_0 + A\sin((2\cdot\pi\cdot f)\cdot t + \varphi_0) \\ y = y_0 \pm v_w\cdot t + (R + h_{nm})\cdot\sin(\theta_{oj} - w\cdot t) \\ z = R - d - (R + h_{nm})\cdot\cos(\theta_{oj} - w\cdot t) \end{cases} \quad (2-1)$$

where x_0 and y_0 are the initial distances between the {O} and {G} origins in x and y directions. A and f are the ultrasonic amplitude and frequency, t is the time, φ_0 is the initial phase of ultrasonic vibration, v_w is the velocity of the workpiece, R is the radius of the grinding wheel, θ_{oj} is the initial angle of the jth row of the grinding wheel array, w is the angular velocity of the grain, and d is the depth of cut. The grinding process is actually a material removal process, which involves the crush of the abrasive grains, elastic plastic deformation, and so on. In order to reduce the complexity of the analysis, the following assumptions are adopted in the modeling process:

1. The calculated depth of cut is the actual depth of cut in the grinding process.
2. The side flow and built-up edge phenomena are not considered in the grinding process.
3. The workpiece material in contact with the cutting edge of the abrasive grains is completely removed when the grinding wheel is feeding.

As shown in Fig. 4, the origin of the workpiece surface coordinate system G-xyz is the highest point of the original workpiece. The workpiece surface is divided into rectangular grids with a definite resolution. The matrix $[g_{ij}]$ represents the height of the rectangular grid with the subscripts i and j corresponding to the positions of the rectangular grid in the x and y directions.

When a discrete data point passes the workpiece surface, the envelope trajectory of the discrete data point is positioned in the rectangular grids of the workpiece surface, and then, the minimum grid heights of different grids are calculated. If the height of the envelope trajectory is higher than the initial height of the rectangular grid, the rectangular grid cannot be cut by this discrete data point. Otherwise, the rectangular grid can be cut, and the initial height of the grid is replaced by the height of the envelope trajectory. The schematic diagram is shown in Fig. 5.

Through the above steps, the envelope trajectory height of all the discrete data points can be calculated, and the minimum envelope trajectory height is taken as the final height of each rectangular grid to finally get the topography of the workpiece surface. The procedures for generation of the micro workpiece surface can be summarized as follows:

(1) The envelope trajectory of a discrete data point is determined according to the input process conditions.
(2) The envelope trajectory is mapped on the workpiece surface.
(3) The minimum value of the envelope trajectory positioned on each rectangular grid is obtained.

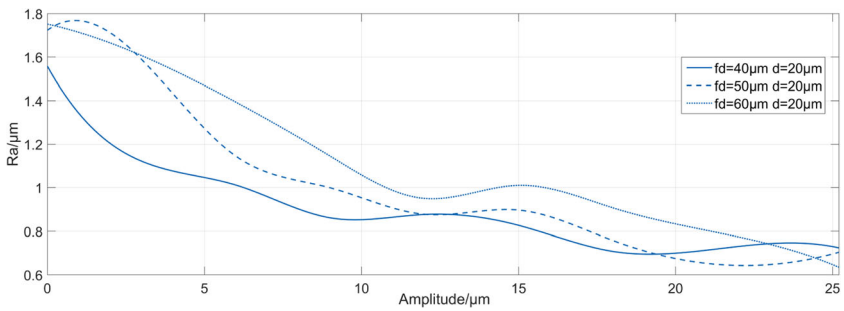

Fig. 12 Variations of surface roughness under different dressing leads ($d = 20$ μm)

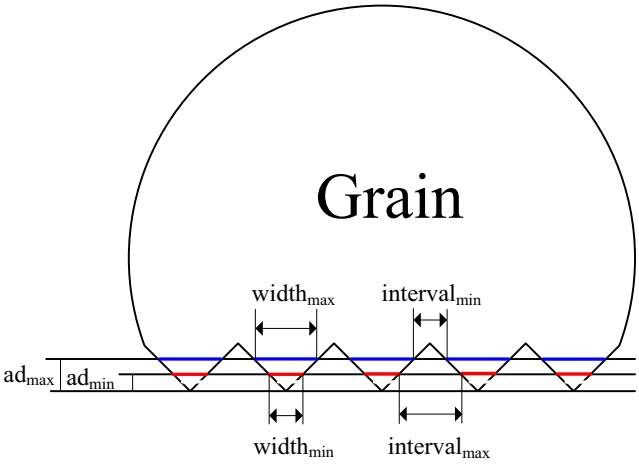

Fig. 13 Effects of depth of cut on cutting edges in UAG and CG

(4) If the minimum height of the envelope trajectory is smaller than the initial height of the rectangular grid and the initial height of the grid is replaced by the height of the envelope trajectory.
(5) The heights of all rectangular grids are obtained by following these steps to get the final workpiece topography.

As can be seen from the above section, ultrasonic amplitude, feed depth, and dressing lead are the most important processing parameters. Other specific processing parameters are shown in Table 1.

Figures 6 and 7 show the UAG workpiece surface under different processing parameters. It is found that the workpiece surface roughness decreases and the width of the grinding trajectory increases with the increase of the ultrasonic grinding amplitude.

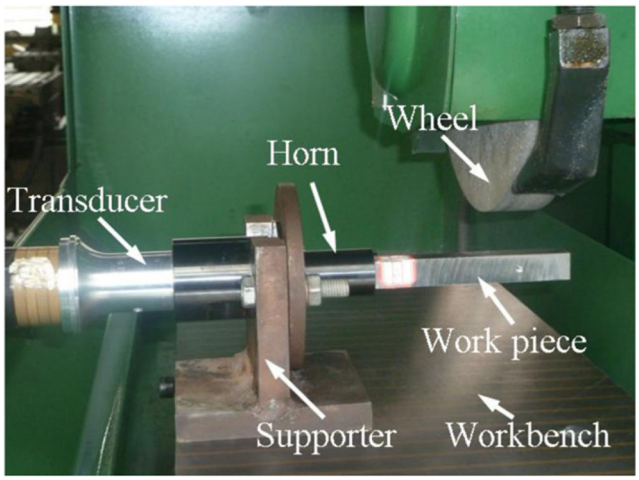

Fig. 14 Experimental setup for the UAG tests

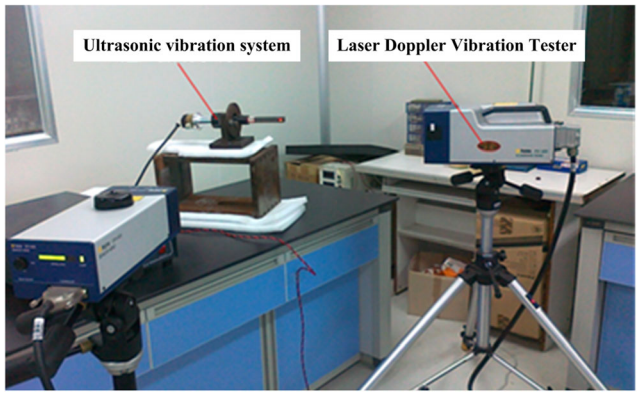

Fig. 15 Ultrasonic amplitude measurement equipment

4 Research on the matching relationship of processing parameters

4.1 Matching relationship of processing parameters by simulation

The roughness is calculated from the workpiece surface obtained in the preceding section. The specific changes are shown in Figs. 8, 9, 10, 11, and 12. It can be observed from the figures that there is little or even adverse effect in terms of UAG surface roughness optimization when the ultrasonic amplitude reaches a certain value, indicating that the ultrasonic amplitude plays a critical role in the ultrasonic grinding surface.

The influence of ultrasonic amplitude on surface roughness with different dressing leads is shown in Fig. 8. As can be seen from the figure, the increment of ultrasonic amplitude causes a decrease of surface roughness in a general trend. When the ultrasonic amplitude is over 13 μm, however, there is only a slight decrease of surface roughness with the increase of ultrasonic amplitude. It worth

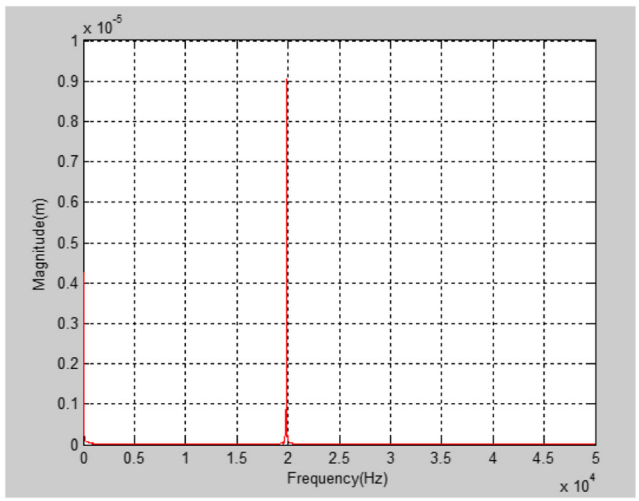

Fig. 16 Ultrasonic amplitude measurement result

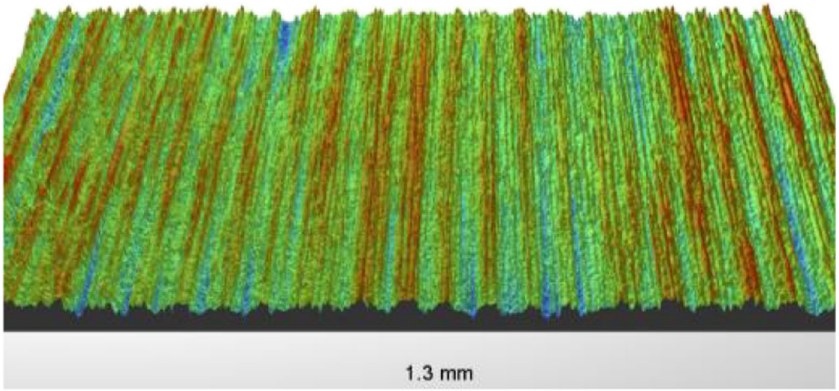

Fig. 17 The measured grinding workpiece surface ($f_d = 50$ μm/r, $A = 0$ μm, and $d = 20$ μm)

noting that there is even a slight increase of the surface roughness for the 40-μm dressing lead when the ultrasonic amplitude is larger than 20 μm. The grinding surface roughness with a 50-μm dressing lead begins level off when the ultrasonic amplitude reaches 23 μm.

Similar step-by-step analysis is carried out for Figs. 9, 10, 11, and 12. Based on the abovementioned matching relationship between UAG surface roughness and dressing lead, feed depth, and ultrasonic amplitude, we found that the decline trend of surface roughness is not obvious when the ultrasonic amplitude reaches a certain value. Therefore, the ultrasonic amplitude with little optimization or improvement effect on surface roughness is defined as the critical ultrasonic amplitude, which is used to reflect the reasonable setting value of ultrasonic amplitudes in ultrasonic grinding.

According to Figs. 8, 9, 10, 11, and 12, the critical ultrasonic amplitude A_{key} can be empirically expressed as a function of the depth of cut d and the dressing lead f_d by $A_{key} = f_d/4 + (18.5 - d)$.

The abrasive grains play a decisive role in the grinding process. Therefore, the analysis of the abrasive grain cutting edge with different cutting depths can reflect the grinding situation. It can be found from Fig. 13 that the width of the cutting edges in common grinding becomes larger as the depth of cut increases. This leads to a larger grooves and thus results in an increase of the surface roughness. Under normal grinding, a smaller dressing lead leads to a smaller distance between the abrasive grain cutting edges, a more uniform grinding surface, and a smaller surface roughness.

Ultrasonic grinding with a smaller dressing lead can also result in a smaller distance between abrasive grain cutting edges. However, unlike the common grinding, the trajectories of adjacent cutting edges are staggered with the aid of axial ultrasonic vibration. Although a larger depth of cut enlarges the cutting edge width, the distance of adjacent cutting edges becomes smaller and the trajectory interference is increased, thereby reducing the workpiece surface roughness. However, the optimization effect on surface roughness by increasing the ultrasonic amplitude gradually weakens as the ultrasonic amplitude increases above a certain value when the most effective interference of adjacent cutting edges occurs. At the same time, the coefficient in front of the depth of cut in the matching relationship between ultrasonic-assisted grinding parameters is closely correlated with the morphology of single-point diamond pens, because it directly determines the sharpness of the cutting edge, thus affecting the relationship between the depth of feed and the cutting edge.

4.2 Experimental analysis and comparison

The experimental device (mechanical surface grinding machine M7130) shown in Fig. 14 is used to validate the

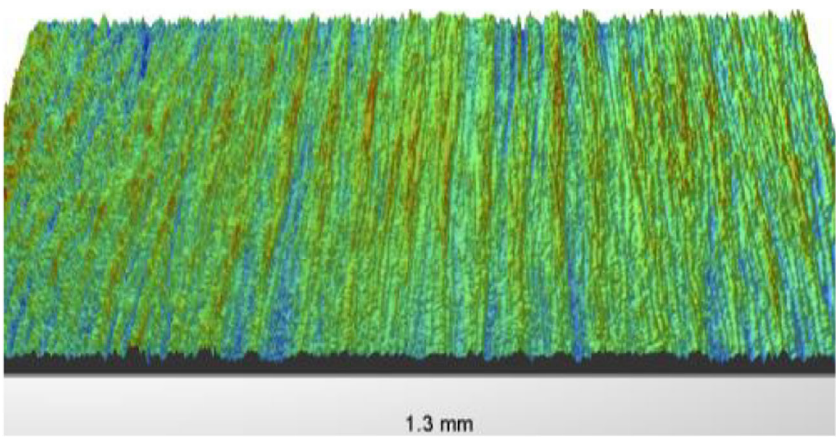

Fig. 18 The measured grinding workpiece surface ($f_d = 50$ μm/r, $A = 9$ μm, and $d = 20$ μm)

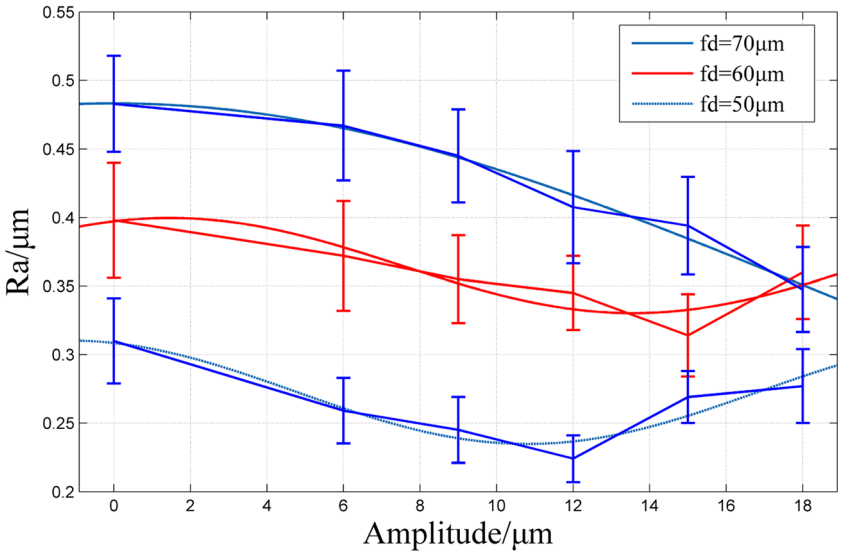

Fig. 19 Variation of surface roughness under different dressing leads ($d = 20$ mm)

simulation results. The experimental details are shown in Table 1. The surface roughness is measured by a Taylor-Hobson Surtronic 3+ profilometer with a cutoff length of 0.8 mm and a test length of 5 mm. Each test is repeated at least three times to obtain the average value of surface roughness. The 3D topography of the ground surface is measured using a Veeco Wyko NT9100 white light interferometer. The German Polytec laser Doppler vibrometer is used to measure the system ultrasonic amplitude (Fig. 15). The amplitude measurement results are shown in Fig. 16.

Figures 17 and 18 show the measured common and ultrasonic-assisted grinding surfaces with an ultrasonic amplitude of 9 μm. It can be found that the cutting edge trajectories interfere with each other and the width of the workpiece grooves increases with the increase of ultrasonic amplitude, which is in accordance with the simulation results.

Experimental tests are conducted with dressing leads of 50 μm, 60 μm, and 70 μm. The ultrasonic amplitude varies from 0 to 18 μm. The depth of cut is set at 20 μm. Figure 19 shows the vibration of surface of roughness at various ultrasonic amplitudes and dressing leads. The measured surface roughness at different dressing leads exhibits similar characteristic, i.e., there is an obvious drop of roughness, while it starts to rise as the ultrasonic amplitudes reach 11 μm and 13.5 for the dressing leads of 50 μm and 60 μm, respectively. These results are in good agreement with the results calculated from the formula of numerical simulation, i.e., $A_{key} = f_d/4 + (18.5 - d)$, which further validates the coupling relationship between the processing parameters in ultrasonic grinding.

5 Conclusions

1. The concept of critical ultrasonic amplitude is proposed, and the coupling relationship between critical ultrasonic amplitude A_{key} and depth of cut d as well as dressing lead f_d is obtained. The numerical results are in good agreement with the experimental results.
2. The inherent physical meaning of the coupling relationship between the machining parameters is explained from the effect of the single abrasive grain cutting edge on the workpiece topography. This deepens our understanding of the effect of machining parameters on the workpiece morphology exerted by cutting edges in UAG, thus providing theoretical support for the optimization of processing parameters.
3. The matching relationship between the three processing parameters of UAG is investigated, which lays the foundation for further optimization of the gear surface roughness in UAG.

Funding information This study received financial supports from the National Key R&D Program of China through Grant No. 2017YFB1300700; the National Natural Science Foundation of China (NSFC) through Grant Nos. 51535012, 51705542, and U1604255; and Key Research and Development Project of Hunan Province through Grant No. 2016JC2001.

References

1. Shao W, Li XS, Sun Y, Huang H, Tang JY (2018) An experimental study of temperature at the tip of point-attack pick during rock cutting process. Int J Rock Mech Min Sci 107:39–47
2. Shao W, Li XS, Sun Y, Huang H (2017) Parametric study of rock cutting with SMART*CUT picks. Tunnel Undergr Space Technol 61:134–144
3. Qi H, Xie Z, Hong T, Wang YY, Kong FZ, Wen DH (2017) CFD modelling of a novel hydrodynamic suspension polishing process

for ultra-smooth surface with low residual stress. Powder Technol 317:320–328
4. Qi H, Wen DH, Lu CD, Li G (2016) Numerical and experimental study on ultrasonic vibration-assisted micro-channelling of glasses using an abrasive slurry jet. Int J Mech Sci 110:94–107
5. Long YY, Li YL, Sun J, Ille I, Li JF, Twiefel J (2018) Effects of process parameters on force reduction and temperature variation during ultrasonic assisted incremental sheet forming process. Int J Adv Manuf Technol 97:13–24
6. Li DG, Tang JY, Chen HF, Shao W (2018) Study on grinding force model in ultrasonic vibration-assisted grinding of alloy structural steel. Int J Adv Manuf Technol. https://doi.org/10.1007/s00170-018-2929-2
7. Liao DR, Shao W, Tang JY, Li JP, Tao X (2018) Numerical generation of grinding wheel surfaces based on time series method. Int J Adv Manuf Technol 94:561–569
8. Liao DR, Shao W, Tang JY, Li JP (2018) An improved rough surface modeling method based on linear transformation technique. Tribol Int 119:786–794
9. Zhou WH, Tang JY, Chen HF, Shao W, Zhao B (2019) Modeling of tooth surface topography in continuous generating grinding based on measured topography of grinding worm. Mech Mach Theory 131:189–203
10. Zhou WH, Tang JY, Chen HF, Zhu CC, Shao W (2018) Modeling of tooth surface topography in continuous generating grinding based on measured topography of grinding worm. Int J Mech Sci 144:639–653
11. Tawakoli T, Azarhoushang B (2009) Effects of ultrasonic assisted grinding on CBN grinding wheels performance. ASME Int Manuf Sci Eng Conf 2:209–214
12. Tawakoli T, Azarhoushang B (2008) Influence of ultrasonic vibrations on dry grinding of soft steel. Int J Mach Tools Manuf 48(14): 1585–1591
13. Nik MG, Movahhedy MR, Akbari J (2012) Ultrasonic-assisted grinding of Ti6Al4 V alloy. Procedia CIRP 1:353–358
14. Chen HF, Tang JY, Shao W, Zhao B (2018) An investigation on surface functional parameters in ultrasonic-assisted grinding of soft steel. Int J Adv Manuf Technol 97:2697–2702
15. Chen HF, Tang JY, Shao W, Zhao B (2018) An investigation of surface roughness in ultrasonic assisted dry grinding of 12Cr2Ni4A with large diameter grinding wheel. Int J Precis Eng Manuf 19(6): 929–936
16. Wang Y, Lin B, Wang S, Cao X (2014) Study on the system matching of ultrasonic vibration assisted grinding for hard and brittle materials processing. Int J Mach Tools Manuf 77:66–73
17. Wang Y, Lin B, Cao X, Wang S (2014) An experimental investigation of system matching in ultrasonic vibration assisted grinding for titanium. J Mater Process Technol 214(9):1871–1878
18. Chen HF, Tang JY, Lang XJ, Huang YL, He YH (2014) Influences of dressing lead on surface roughness of ultrasonic-assisted grinding. Int J Adv Manuf Technol 71(9–12):2011–2015
19. Ding H, Tang JY, Shao W, Zhou YS, Wan GX (2017) Optimal modification of tooth flank form error considering measurement and compensation of cutter geometric errors for spiral bevel and hypoid gears. Mech Mach Theory 118:14–31
20. Shao W, Ding H, Tang JY, Peng SD (2018) A data-driven optimization model to collaborative manufacturing system considering geometric and physical performances for hypoid gear product. Robot Comput Integr Manuf 54:1–16
21. Shao W, Ding H, Tang JY, Peng SD (2018) Data-driven operation and compensation approaches to tooth flank form error measurement for spiral bevel and hypoid gears. Measurement 122:347–357
22. Ding H, Tang JY, Shao W, Peng SD (2018) An innovative determination approach to tooth compliance for spiral bevel and hypoid gears by using double-curved shell model and Rayleigh–Ritz approach. Mech Mach Theory 130:27–46
23. Jiang JL, Ge PQ, Bi WB, Zhang L, Wang DX, Zhang Y (2013) 2D/3D ground surface topography modeling considering dressing and wear effects in grinding process. Int J Mach Tools Manuf 74:29–40
24. Saad A, Bauer R, Warkentin A (2010) Investigation of single-point dressing overlap ratio and diamond-roll dressing interference angle on surface roughness in grinding. Trans Can Soc Mech Eng 34(2): 295–308
25. Oliveira JFG, Bottene AC, Franca TV (2010) A novel dressing technique for texturing of ground surfaces. Ann CIRP 59(1):361–364
26. Malkin S (1989) Grinding technology: theory and applications of machining with abrasives, 1st edn. Ellis Horwood, New York
27. Zhou X, Xi F (2002) Modeling and predicting surface roughness of the grinding process. Int J Mach Tools Manuf 42(8):969–977
28. Malkin S (2008) Grinding technology: theory and applications of machining with abrasives, 2nd edn. Industrial Press Inc.